Energy Engineering

Tech Science Press

http://doi.org/10.32604/ee.2026.087533

ARTICLE

Prescribed Performance H_∞ Control of Distributed Energy Resources with Multi-Agent Coordination and Its Application in Microgrids

Dongmei Wang[1,2], Huixin Song[1,2,*] and Yanze Song[3]

[1]Skills Training Center of State Grid Jibei Electric Power Co., Ltd., Baoding, China
[2]Department of Power Generation and Transformation Engineering, Baoding Technical College of Electric Power, Baoding, China
[3]Department of Electrical Engineering, North China Electric Power University, Baoding, China
*Corresponding Author: Huixin Song. Email: songhuixinm@163.com

Received: 18 June 2026; Accepted: 08 July 2026; Published: 12 November 2026

ABSTRACT: This paper addresses the H_∞ consensus problem for a network of distributed energy resources (DERs) subject to edge-based communication disturbances. Prescribed performance control is adopted to improve the convergence and robustness of phase synchronization of DERs in a microgrid. Unlike traditional consensus control approaches, we consider DERs in microgrids that are subject to communication disturbances—a common issue in the monitoring and coordination of such systems. To this end, we propose a prescribed performance control protocol that incorporates error transformation techniques and prescribed performance constraints. By utilizing Lyapunov stability theory, we demonstrate that H_∞ consensus of the DERs is achieved with prescribed performance, which effectively suppresses communication disturbances. Finally, simulation results verify the feasibility and validity of the theoretical findings.

KEYWORDS: Prescribed performance control; H_∞ control; distributed energy resources; multi-agent systems; phase synchronization; communication disturbance

1 Introduction

Cooperative control is one of the most widely studied topics today, encompassing various control forms such as consensus, clustering, grouping, and formation. Its industrial applications are also extensive, including state monitoring in multi-sensor systems, attitude alignment in multi-satellite systems, and cooperative power management of distributed energy resources in microgrids. Some classic research findings on cooperative control problems of multi-agent systems have been published in the literature, such as [1,2]. Based on the classification of the dynamic systems studied, we can see that common systems include first-order dynamic systems, second-order dynamic systems, higher-order dynamic systems, linear dynamic systems, and nonlinear dynamic systems [3].

Reviewing the above literature, we can see that consensus, as a classic research topic in the field of distributed control, provides fundamental theoretical support and research paradigms for other forms of research [4]. Due to its excellent scalability, the consensus problem also has high research value in building large-scale distributed energy systems [5,6]. Generally, consensus problems focus more on the asymptotic stability of system states [7], while typically neglecting transient characteristics such as overshoot, convergence rate, and steady-state error. However, in the response process involving multiple distributed energy resources (DERs), the transient performance of dynamic processes is crucial and directly

Copyright © 2027 The Authors. Published by Tech Science Press. This work is licensed under a Creative Commons Attribution 4.0 International License, which permits unrestricted use, distribution, and reproduction in any medium, provided the original work is properly cited.

affects the stable operation of the system. To address this issue, reference [8] first proposed the prescribed performance control (PPC) method. This method restricts the evolution trajectory of state errors (such as power allocation errors) within a prescribed performance region, thereby ensuring the lower bound of convergence rate, the upper bound of overshoot, and the satisfaction of the steady-state error residual set.

Furthermore, Prescribed Performance Control has been applied in many fields, such as robot system control [9], large vehicle platooning [10], and unmanned aerial vehicle (UAV) system [11]. Next, we will review typical application scenarios of Prescribed Performance Control in microgrids. For DERs in microgrids with phase synchronization dynamics that can be simplified to a single integrator (such as an active power control loop), the PPC protocol proposed by Chen et al. [12] provides a framework for achieving coordinated power control. As an unavoidable dynamic disturbance factor in the operation of distributed energy systems, communication disturbance poses a significant challenge to the stability of system cooperation performance. In cluster systems composed of multiple DERs, factors such as channel noise, packet loss, and latency jitter can all lead to communication disturbance, which is essentially the superposition effect of non-ideal factors during information interaction. This disturbance not only disrupts the consensus of power allocation among DERs, but also seriously threatens the stable operation of the microgrid.

Recent studies have applied prescribed performance control to microgrid coordination and secondary control problems. Soofi et al. [13] proposed a prescribed performance control strategy for isolated multi-agent direct current (DC) microgrids, showing that PPC can constrain transient responses in microgrid coordination. Zaery et al. [14] developed a predefined-time prescribed-performance control method for DC microgrid clusters, with emphasis on prescribed convergence time. Yuan et al. [15] introduced prescribed performance into secondary control of DC microgrids, mainly for voltage regulation, while Li et al. [16] studied prescribed-time consensus control for DC microgrids. These studies confirm the value of prescribed transient performance constraints in microgrid control. However, they do not explicitly address L_2-bounded disturbances in communication links or integrate prescribed performance with an H_∞ disturbance attenuation framework.

Robust consensus and H_∞ control have also been investigated for microgrid applications. Dong et al. [17] proposed a data-driven distributed H_∞ current-sharing consensus optimal control method for DC microgrids. Raeispour et al. [18] studied resilient H_∞ consensus-based control for autonomous alternating current (AC) microgrids with uncertain time-delayed communications. Zhou et al. [19] developed an event-triggered H_∞ consensus current-sharing control method for DC microgrids under uncertainties, and Zhao et al. [20] proposed a Kalman-filter-based robust consensus secondary control method considering communication delays and noises. These works improve robustness against uncertainty, delay, or communication noise, but they do not enforce prescribed transient performance bounds through PPC.

The above discussion reveals two remaining gaps. First, existing PPC-based microgrid consensus studies usually focus on transient constraints or prescribed convergence time, but they seldom provide an H_∞ robustness guarantee for communication-link disturbances. Second, existing H_∞ microgrid consensus studies mainly address robustness and disturbance attenuation, but they do not constrain the transient evolution of edge errors within a prescribed performance envelope. These gaps motivate the prescribed-performance H_∞ consensus framework developed in this paper.

To address these issues, this paper studies the cooperative control problem of DER clusters under communication disturbance. The core contribution of this paper is to propose a pre-set performance H_∞ distributed control strategy based on a multi-agent system. This strategy combines the transient performance management capability of PPC with the disturbance suppression capability of H_∞ control,

aiming to ensure that the networked equipment cluster (1) achieves precise phase synchronization; (2) the transient performance of the entire dynamic process meets the pre-set requirements; and (3) has strong robustness against bounded disturbance in the communication channel. Theoretical analysis and simulation results show that the proposed method can significantly improve the dynamic quality and stability of the system under non-ideal communication environments, providing a solid theoretical basis for the engineering application of DER clusters in a microgrid.

To ensure clarity and ease of reference throughout the paper, the next section lists all key abbreviations along with their full terms.

2 Background and Problem Statement

2.1 Graph Theory

An undirected graph $\mathcal{G} = \{\mathcal{V}, \mathcal{E}\}$ with N nodes and M edges is used to represent the communication graph, where the node set $\mathcal{V} = \{1, 2, \cdots, N\}$ and edge set $\mathcal{E} \subset \mathcal{V} \times \mathcal{V}$. The set $\mathcal{N}_i = \{j \in \mathcal{V} : (i, j) \in \mathcal{E}\}$ denotes the neighbors of node i. If $j \in \mathcal{N}_i$, there exists an edge $l \in \mathcal{H}$ linked between node j and i, with $\mathcal{H} = \{1, \cdots, M\}$ being edge set. Let us define $\mathcal{L}$ as the Laplacian matrix of $\mathcal{G}$. The incidence matrix is defined as $B = [b_{il}] \in \mathcal{R}^{N \times M}$, with rows and columns indexed by the node $i \in \mathcal{V}$ and edge $l \in \mathcal{H}$, respectively. Given the tree graph $\mathcal{G}$, the edge Laplacian matrix $\mathcal{L}_e = B^\top B$ is positive definite. If $\mathcal{G}$ is connected, $\mathcal{L}_e$ is positive semi-definiteness [12].

2.2 System Description

Clustered operation of DERs in a microgrid utilizes a collaborative control architecture built upon a communication network, in which the dynamic characteristics of its core control loops can often be simplified to a first-order integrator. Based on this, we model a cluster of N grid-connected converters as a multi-agent system, where the dynamic model of the i-th agent is described as follows:

$$\dot{x}_i(t) = u_i(t) + \sum_{l=1}^{M} b_{il} w_l(t), \ i \in \mathcal{V}, \tag{1}$$

where $x_i(t)$ and $u_i(t) \in \mathcal{R}$ represent the core state variable and distributed control input of agent i, respectively. In the context of collaborative control of network-type equipment, $x_i(t)$ can be specifically characterized as the output voltage phase angle of device i or its integral with respect to the system frequency deviation; correspondingly, $u_i(t)$ is the phase angle or frequency adjustment command calculated according to the distributed control protocol. $wl(t) \in L_2[0, +\infty)$ is the disturbance acting on the communication edge l, used to characterize channel noise, packet loss, and random disturbance in the communication edge under the complex electromagnetic environment of the substation.

The first-order integrator model in (1) should be interpreted as a high-level coordination-layer abstraction rather than a full inverter-level dynamic model. This abstraction is commonly used when the inner current, voltage, and power control loops of DERs are sufficiently faster than the secondary coordination layer. In such cases, the inner loops track the coordination commands on a shorter time scale, while the distributed controller determines the slow coordination dynamics among DER units. Similar reduced-order descriptions have been adopted in microgrid consensus and secondary-control studies, including inverter consensus control and PPC-based DC microgrid secondary control [7,15].

The validity of this abstraction relies on several operating conditions. The inner-loop bandwidth should be significantly higher than the update rate of the coordination layer; the communication graph

should remain connected during the considered interval; the communication disturbance should have finite energy; and the DER operating point should not change abruptly. When the microgrid operates under weak-grid conditions, when inner-loop dynamics slow down, or when persistent communication failures change the network topology, a higher-order DER model with explicit inverter and delay dynamics would be required. These extensions are beyond the scope of the present work and will be investigated in future studies.

The L_2 norm boundedness assumption is a standard and theoretically tractable framework in H_∞ control, encompassing a wide range of practical disturbances with finite energy, including (but not limited to) sinusoidal noise, bounded random noise, and even impulsive or burst-type disturbances provided their total energy is finite. Such disturbances can be considered as having finite energy in physical reality, i.e., bounded L_2 norm.

The L_2-bounded disturbance model $w_l(t)$ serves as a unified, energy-bounded representation for various communication imperfections. Specifically:

(1) Additive channel noise (e.g., Gaussian or bounded noise) maps directly to $w_l(t)$ as a continuous signal with finite energy.
(2) The aggregated effect of intermittent packet loss over time can be equivalently represented by a piecewise L_2 signal, modeling the error induced during loss intervals.
(3) Burst disturbances with bounded amplitude and duration naturally satisfy the finite-energy (L_2) condition.

This model is therefore effective for robustness analysis against a broad class of finite-energy perturbations. However, it is important to note its limitations: it does not explicitly capture the dynamics of time-varying delays or model persistent link failures that alter the network topology. These aspects, while beyond the scope of this initial study, are important considerations for future extensions towards more specific communication fault models.

The collaborative control objective of the system is reflected in the relative relationships between the states of the devices. Let $y = [y_1, y_2, \cdots, y_M]^\top$ be a stacked form of relative output vectors, where $y_l(t) = x_i(t) - x_j(t)$ represents the relative state corresponding to the communication edge $l \in \mathcal{H}$ connecting agents i and j. It is easy to see that $y = B^\top x$, where $x = [x_1, x_2, \cdots, x_N]^\top$.

2.3 Prescribed Performance Control

Prescribed transient performance is achieved if the relative positions y_l, $l \in \mathcal{H}$ evolve within prescribed performance regions,

$$-\rho_l(t) < y_l(t) < \rho_l(t), \quad \forall t \geq 0 \tag{2}$$

where $\rho_l(t)$ is smooth, bounded and decreasing performance function associated with $y_l(t)$. Partly inspired by [21,22], one can select performance function

$$\rho_l(t) = (\rho_l^0 - \rho_l^\infty)e^{-\lambda t} + \rho_l^\infty \tag{3}$$

with ρ_l^0, ρ_l^∞, and λ appropriately chosen positive constants, for $l = 1, \cdots, M$. In fact, $\rho_l(t)$ satisfies:

(1) $\rho_l(0) = \rho_l^0 > \rho_l^\infty$;
(2) $\lim_{t\to 0} \rho_l(t) = \rho_l^\infty > 0$; and
(3) $\rho_l(t)$ is decreasing and $\rho_l(t)$ is uniformly continuous.

Remark 1: *It follows from* (3) *that* $\rho_l(t)$ *is smooth and decreasing for* $t \geq 0$ *. Comparing with the traditional performance control methods, the proposed performance function* (3) *has the property that it can achieve prescribed performance convergence. There are three adjustable positive parameters* ρ_l^0, ρ_l^∞, *and* λ *in* (3).

Generally speaking, the value of λ *decides the traced profile of performance function, and it is used to determine the minimum convergence rate of the relative positions* $y_l(t)$. *The larger the value of* λ, *the faster convergent rate. The constants* ρ_l^∞ *are used to determine an arbitrarily small residual set of relative positions* $y_l(t)$. *In fact, the prescribed performance specifications are imposed in advance according to the practical requirement and thus* $\rho_l(t)$, $l \in \mathcal{H}$ *are specified a priori. By choosing the more suitable* $\rho_l(0)$, *the maximum overshoot is less than* $\rho(0)$. *For any unknown but bounded relative positions* $y_l(0)$, *the following inequality holds*

$$-\rho_l(0) < y_l(0) < \rho_l(0), \quad \forall t \geq 0.$$

In this case, the initial errors $y_l(0)$ *are usually known accurately. Furthermore, one has*

$$\dot{\rho}_l(t) = -\lambda(\rho_l^0 - \rho_l^\infty)e^{-\lambda t}, \ \forall t \geq 0. \tag{4}$$

It follows that $\dot{\rho}_l(t)$ *is uniformly continuous with* $\min\limits_{t\geq 0, l\in\mathcal{H}}\{\dot{\rho}_l(t)\} = -\lambda(\rho_l^0 - \rho_l^\infty)$ *and* $\max\limits_{t\geq 0, l\in\mathcal{H}}\{\dot{\rho}_l(t)\} = 0$.

Remark 2: *Providing clear guidelines for tuning the prescribed performance function (PPF) parameters is essential for the implementation of the proposed control scheme. The prescribed performance function is defined as* $\rho_l(t) = (\rho_l^0 - \rho_l^\infty)e^{-\lambda t} + \rho_l^\infty$, $t \geq 0$, *where* $\rho_l^0 > 0$, $\rho_l^\infty > 0$, *and* $\lambda > 0$ *are the key design parameters. Their practical selection can be guided by the following considerations:*

(1) *Initial bound* ρ_l^0*: This parameter represents the maximum allowable error at* $t = 0$. *It should be chosen based on the expected initial synchronization error among the distributed energy resources (DERs), which can be estimated from typical operating conditions or historical data in the microgrid.*

(2) *Steady-state bound* ρ_l^∞*: This parameter defines the ultimate accuracy of the synchronization. It should be selected according to the required steady-state performance specifications, such as the permissible phase or frequency deviation in the microgrid standards.*

(3) *Convergence rate* λ*: This parameter dictates the speed at which the performance bounds shrink from* ρ_l^0 *to* ρ_l^∞. *A larger* λ *leads to faster transient convergence but may require higher control effort. A practical way to choose* λ *is to relate it to a desired settling time* T_s. *For instance, if we require the performance bound to reach a fraction* ϵ *(e.g.,* $\varepsilon = 0.05$*) of its initial deviation by* T_s, *then* λ *can be approximated by:* $\lambda \approx \frac{1}{T_s}\ln\left(\frac{\rho_l^0 - \rho_l^\infty}{\varepsilon\rho_l^0}\right)$.

Furthermore, we emphasize that the selection of these parameters should also account for the physical constraints of the DER inverters, such as current and voltage limits. In practice, an iterative tuning process based on simulation studies is recommended to finalize the parameters, ensuring a balance between desirable transient performance and feasible control effort.

By defining the normalized relative positions $\hat{y}_l(t) = \frac{y_l(t)}{\rho_l(t)}$ and due to $\rho_l^0 \geq \hat{y}_l(0)$, the prescribed performance regions are simply written as $\hat{y}_l(t) \in D_{\hat{y}_l}$, $\forall t \geq 0$, with open sets $D_{\hat{y}_l}$, $l = 1, \cdots, M$ defined as follows,

$$D_{\hat{y}_l} \triangleq \{\hat{y}_l(t) \in \mathcal{R} \ : \ \hat{y}_l(t) \in (-1, 1)\}, \quad \forall t \geq 0.$$

For notation convenience, we define $D_{\hat{y}} \triangleq D_{\hat{y}_1} \times D_{\hat{y}_2} \times \cdots \times D_{\hat{y}_M}$, with $\hat{y} = [\hat{y}_1, \cdots, \hat{y}_M]^\top$ and $\rho(t) = \text{diag}\{\rho_1(t), \cdots, \rho_M(t)\}$.

To proceed, an error transformation function is introduced to achieve the prescribed performance specifications. More specifically, we define the transformation function as follows

$$\varepsilon_l(\hat{y}_l) = \ln\left(\frac{1+\hat{y}_l}{1-\hat{y}_l}\right) \tag{5}$$

where the transformation functions are smooth and strictly increasing bijective mapping

$$\varepsilon_l : (-1, 1) \to (-\infty, \infty),$$

with

$$\varepsilon_l(0) = 0 \tag{6}$$

for $l = 1, \cdots, M$.

Taking the time derivative of (5), we have

$$\dot{\varepsilon}_l(\hat{y}_l) = J_l(\hat{y}_l, t)[\dot{y}_l + \alpha_l(t) y_l] \tag{7}$$

with $J_l(\hat{y}_l, t) = \frac{2}{1-\hat{y}_l^2} > 0$ and $\alpha_l(t) \triangleq -\frac{\dot{\rho}_l(t)}{\rho_l(t)} > 0$. Owing to the property (6), the following inequalities hold [9,12]

$$\varepsilon^\top(\hat{y}) J(\hat{y}, t) y \geq \zeta_1 \|\varepsilon(\hat{y})\|^2, \ \varepsilon^\top(\hat{y}) J(\hat{y}, t) y \geq \zeta_2 \|\hat{y}\|^2 \tag{8}$$

for positive constants ζ_1 and ζ_2.

A typical choice for $\rho_l(t)$ is $\rho_l(t) = (\rho_l^0 - \rho_l^\infty)e^{-\lambda t} + \rho_l^\infty$, where $\rho_l^0 > \rho_l^\infty > 0$ and $\lambda > 0$. The key property of this function is that it mathematically prescribes the transient performance: it explicitly defines an exponentially decaying envelope with a guaranteed minimum convergence rate (determined by λ) and a maximum steady-state error bound (ρ_l^∞). The condition $\rho_l^0 > |y_l(0)|$ ensures the initial error is within the envelope. Unlike traditional asymptotic control that only ensures $\lim_{t\to\infty} y_l(t) = 0$, the framework of Ineq. (2) enforces strict bounds on $y_l(t)$ for all time $t \geq 0$. This is achieved by transforming the constrained error dynamics into an equivalent unconstrained stabilization problem via a suitable error transformation (e.g., ε_l), which is a core technique in prescribed performance control.

The error transformation is a crucial step to enforce the constraint (2). Defining the normalized error $\hat{y}_l(t) = y_l(t)/\rho_l(t)$, the constraint becomes $-1 < \hat{y}_l(t) < 1$. We then apply a strictly increasing, bijective mapping from $(-1, 1)$ to $\mathcal{R}$, such as the inverse hyperbolic tangent: $\varepsilon_l(t)$. This transformation converts the *constrained* stabilization problem for $y_l(t)$ (within $\pm\rho_l(t)$) into an *unconstrained* stabilization problem for $\varepsilon_l(t)$ (over $\mathcal{R}$). The bijective nature of the mapping guarantees that if the transformed error $\varepsilon_l(t)$ is kept finite (e.g., stabilized to zero), then the original normalized error $\hat{y}_l(t)$ will remain strictly within $(-1, 1)$, thereby ensuring $-\rho_l(t) < y_l(t) < \rho_l(t)$ for all time by construction.

By Barbalat's Lemma and the properties of performance function (3), one can obtain the following property.

Property 1 ([23]): *For the designed performance function (3), there exists some positive constant $\bar{\alpha}$ satisfying the following inequalities*

$$\bar{\alpha} \geq \max_{t\geq 0, l\in\mathcal{H}} \{\alpha_l(t)\}. \tag{9}$$

2.4 Problem Statement

The aim of this paper is, for system (1) with the connected graph $\mathcal{G}$ and the performance function $\rho_l(t)$, $l = 1, \cdots, M$, to design a distributed, prescribed performance control protocol to collaboratively control a DER cluster. The specific problems to be solved are as follows:

(1) Prescribed Performance: relative positions $y_l(t)$ will evolve within performance bounds (2);
(2) Consensus: consensus of all agents can be achieved with $w = 0$, if the following conditions hold

$$\lim_{t\to\infty} y(t) = 0, \quad \text{for system (1)};$$

(3) H_∞ Consensus: system (1) solves H_∞ consensus if consensus is achieved with $w = 0$ and there exists positive constant φ satisfying

$$\int_0^\infty s^\top(t)s(t)dt \leq \varphi \int_0^\infty w^\top(t)w(t)dt \tag{10}$$

for $w \neq 0$ under zero initial condition, where $s = \hat{y}$ for system (1).

For the DER synchronization problem, the relative output $y_l(t)$ (and consequently $\hat{y}_l$) corresponds to the phase angle difference between interconnected DERs. Thus, the H_∞ performance index in (10) specifically bounds the energy of synchronization errors relative to the energy of communication disturbances. This guarantees that the overall synchronization accuracy, a critical operational metric, remains robust against finite-energy communication imperfections.

Lemma 1 ([23]): *For any $\kappa, D > 0$, the following holds:*

$$-\kappa\varepsilon^\top(\hat{y})J(\hat{y}, t)y + D < 0 \tag{11}$$

for all $\|\varepsilon(\hat{y})\| > \bar{\varepsilon}$ and a positive constant $\bar{\varepsilon}$.

Lemma 2 (Schur complement lemma): *Given a matrix $S = \begin{bmatrix} S_{11} & S_{12} \\ S_{21} & S_{22} \end{bmatrix}$ where $S \in \mathcal{R}^{N\times N}$, $S_{11} \in \mathcal{R}^{n\times n}$, $S_{12} = S_{21}^\top$. Then the following conditions are equivalent:*

(1) $S < 0$;
(2) $S_{11} < 0$, $S_{22} - S_{21}S_{11}^{-1}S_{12} < 0$; *and*
(3) $S_{22} < 0$, $S_{11} - S_{12}S_{22}^{-1}S_{21} < 0$.

Lemma 3: *For the given matrix $Q = \begin{bmatrix} \theta\gamma I_N & \theta I_N \\ \theta I_N & I_N \end{bmatrix}$, there exist positive constants γ, θ satisfying $\gamma > \theta$ such that $Q > 0$.*

Proof of Lemma 3: By using Lemma 2, the positive definiteness of matrix Q can be obtained. The proof is completed. □

3 Main Results

This section presents a prescribed performance control protocol for the multi-agent system representing a DER cluster. It is rigorously proven that the proposed protocol fulfills the control objectives stated in Section 2.4, ensuring consensus with prescribed transient and steady-state performance while attenuating communication disturbances.

3.1 Prescribed Performance Control Protocol

In this part, we firstly consider the prescribed performance control problem for first-order multi-agent systems. In particular, the same stability analysis methods are adopted for different communication graphs, i.e., the spanning tree case and connected graph case.

For the system (1), we propose the prescribed performance control protocol as follows

$$u_i(t) = -\sum_{l=1}^{M} b_{il} J_l(\hat{y}_l, t)\varepsilon_l(\hat{y}_l(t)), \tag{12}$$

which is used to drive the state evolution of agent i, $i \in \mathcal{V}$. With $w = [w_1, w_2, \cdots, w_M]^\top$, the multi-agent system (1) with the prescribed performance control protocol (12) is rewritten as

$$\dot{x}(t) = -BJ(\hat{y}, t)\varepsilon(\hat{y}(t)) + Bw(t). \tag{13}$$

Remark 3: *It is important to note that the H_∞ performance objective aims to attenuate the effect of the exogenous communication disturbances $w_l(t)$ on the defined output $s(t)$. The consensus feedback, which relies on the relative measurements $y_l(t)$, is part of the nominal closed-loop dynamics that the controller must stabilize. The design thus inherently manages the trade-off between utilizing $y_l(t)$ for coordination and suppressing the unwanted influence of $w_l(t)$ embedded within the communication channels.*

To proceed, we derive the following main results.

Theorem 1: *Consider the prescribed performance control protocol (12) applied to the multi-agent system (1) with performance function $\rho_l(t)$, $l \in \mathcal{H}$. If the graph $\mathcal{G}$ is connected, then*

(a) relative positions $y_l(t)$ will evolve within performance bounds (2); and
(b) H_∞ consensus is achieved for the multi-agent system (1).

Proof of Theorem 1: The proof consists of three steps, (1) the boundedness of $\varepsilon(\hat{y})$, (2) the stability analysis of the relative positions $y_l(t)$, and (3) H_∞ consensus analysis with the external disturbance. Consider the following potential function

$$V_1(t) = \frac{1}{2}\varepsilon^\top(\hat{y})\varepsilon(\hat{y}) + \frac{\mu}{2}x^\top x \tag{14}$$

with $\mu > \bar{\alpha}$ being an appropriately chosen positive constant. Taking the time derivative of $V_1(t)$ along the trajectories of (13), we obtain

$$\begin{aligned}\dot{V}_1(t) = &-\varepsilon^\top(\hat{y})J(\hat{y}, t)B^\top BJ(\hat{y}, t)\varepsilon(\hat{y}) + \varepsilon^\top(\hat{y})J(\hat{y}, t)B^\top Bw - \hat{y}^\top\dot{\rho}(t)J(\hat{y}, t)\varepsilon(\hat{y}) \\ &- \mu y^\top J(\hat{y}, t)\varepsilon(\hat{y}) + \mu y^\top w.\end{aligned}$$

Given the connected graph $\mathcal{G}$, the matrix $B^\top B$ is positive semidefinite. By using Young's inequality, one has, with $0 < a_1 \leq 1$, $0 < a_2 < \frac{(\mu-\bar{\alpha})\zeta_2}{\mu\|\rho(0)\|^2}$,

$$\varepsilon^\top(\hat{y})J(\hat{y},t)B^\top Bw \leq a_1\|BJ(\hat{y},t)\varepsilon(\hat{y})\|^2 + \frac{\lambda_{\max}(B^\top B)}{4a_1}w^\top w,$$
$$y^\top w \leq a_2 y^\top y + \frac{1}{4a_2}w^\top w.$$

From the above inequalities, we get

$$\begin{aligned}\dot{V}_1(t) \leq & -(1-a_1)\|BJ(\hat{y},t)\varepsilon(\hat{y})\|^2 - (\mu-\bar{\alpha})\hat{y}^\top J(\hat{y},t)\varepsilon(\hat{y}) + \mu a_2 y^\top y \\ & + \frac{\lambda_{\max}(B^\top B)}{4a_1}w^\top w + \frac{\mu}{4a_2}w^\top w.\end{aligned}$$

By inequality (8), one has

$$\begin{aligned}\dot{V}_1(t) \leq & -(\mu-\bar{\alpha})\zeta_2\|\hat{y}\|^2 + \mu a_2\|\rho(0)\|^2\hat{y}^\top\hat{y} + \frac{\lambda_{\max}(B^\top B)}{4a_1}w^\top w + \frac{\mu}{4a_2}w^\top w \\ \leq & -\kappa_1\|\hat{y}\|^2 + \kappa_2 w^\top w\end{aligned}$$

where $\kappa_1 = (\mu-\bar{\alpha})\zeta_2 - \mu a_2\|\rho(0)\|^2$, $\kappa_2 = \frac{\lambda_{\max}(B^\top B)}{4a_1} + \frac{\mu}{4a_2}$. In order to suppress external disturbance, the following two sequential cases are considered.

(1) If $w(t) \equiv 0$, we obtain $\dot{V}_1(t) \leq -\kappa_1\|\hat{y}\|^2 \leq 0$, in turn, $V_1(t) \leq V_1(0)$. Since $\hat{y}(0) \in D_{\hat{y}}$, $V_1(0)$ is finite, and $\varepsilon(\hat{y}) \in \mathcal{L}_\infty$, with $\mathcal{L}_\infty$ being the space of all essentially bounded measurable functions. Further, the boundedness of $\varepsilon(\hat{y})$ indicates that the relative positions $y_l(t)$ will evolve within performance bounds (2). Owing to the boundedness of $\varepsilon(\hat{y})$ and $\dot{\varepsilon}(\hat{y})$, $\ddot{V}_1(t)$ is bounded, that is, $\dot{V}_1(t)$ is uniformly continuous. By applying Barbalat's Lemma, we thus have $\lim_{t\to\infty}\dot{V}_1(t) = 0$, and thus $\lim_{t\to\infty} y(t) = 0$.

(2) If $w(t) \neq 0$, under zero initial condition of multi-agent system (1), we have, with $T > 0$,

$$\begin{aligned}\int_0^T \kappa_1\hat{y}^\top\hat{y}dt &= \int_0^T \left(\kappa_1\hat{y}^\top\hat{y} + \dot{V}_1(t)\right)dt - (V_1(T) - V_1(0)) \\ &= \int_0^T \left(\kappa_1\hat{y}^\top\hat{y} + \dot{V}_1(t)\right)dt - V_1(T) \\ &\leq \int_0^T \left(\kappa_1\hat{y}^\top\hat{y} + \dot{V}_1(t)\right)dt \\ &\leq \kappa_2\int_0^T w^\top w dt.\end{aligned}$$

Hence, letting $T \to \infty$, the closed-loop system (13) can achieve H_∞ consensus. The proof is completed. □

Noting that the connected graph may contain cycles, while the spanning tree graph do not have cycles. As can be seen, the tree graph is a special case of the connected graph. Compared to the existing literature [12], Theorem 1 is also applicable to the spanning tree graph without an additional proof process.

3.2 The Application in Microgrids

In recent years, the advancement of microgrid infrastructure is proceeding at an accelerated pace, concomitant with a growing diversification and sophistication of external disturbance scenarios [24]. Against this backdrop, a large number of DERs need to perform phase synchronization when external disturbances occur. This section will explain how the prescribed performance H_∞ control protocol proposed in Section 3.1 provides a systematic solution for the collaborative operation of DER clusters, the control flowchart in microgrid applications is shown in Fig. 1.

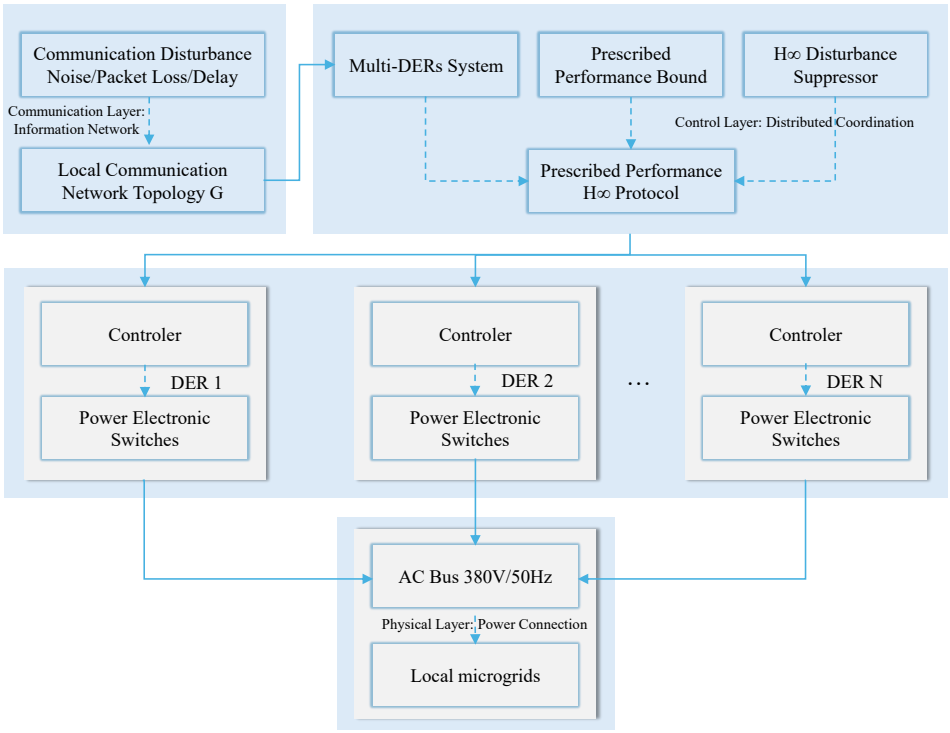


Figure 1: The control flowchart of the application in microgrid.

1. Application Scenarios and System Architecture. Consider a microgrid equipped with multiple DERs, one of whose task is to ensure phase synchronization. We abstract the core control dynamics of each DER (such as virtual synchronous generator (VSG) control) as a first-order integrator model as shown in Eq. (1). Wherein, the state variable $x_i(t)$ represents the power output of the i-th DER, and the control input $u_i(t)$ is a distributed control law based on neighbor information. Devices exchange their operating states through a local communication network $\mathcal{G}$ to achieve coordinated control.

2. Core Control Problem and Theoretical Mapping. The core control problem faced by this cluster is: how to ensure that all DERs achieve rapid phase synchronization in the presence of communication disturbance $w_l(t)$. This problem maps precisely to the prescribed performance H_∞ consensus problem presented in Section 2.4:

Relative Output $y_l(t)$: The relative phase angle between state variables $x_i(t)$ and $x_j(t)$. Its convergence to zero is the mathematical representation of achieving synchronization.

Prescribed Performance $\rho_l(t)$: By applying a performance envelope to $y_l(t)$, the instantaneous phase difference during synchronization can be strictly limited, thereby avoiding damage to the equipment due to excessive transient circulating currents and ensuring a fast and smooth synchronization process.

H_∞ Performance: The protocol's built-in H_∞ disturbance suppression capability effectively attenuates communication noise and delay introduced by the complex electromagnetic environment of substations, ensuring the robustness of the collaborative control system under non-ideal communication conditions. Mathematically, the H_∞ consensus condition (10) guarantees that the cumulative squared phase angle error (i.e., $\int_0^\infty \hat{y}^\top \hat{y} dt$) is proportionally bounded by the energy of the disturbances. This provides a worst-case assurance on synchronization precision.

3. Closed Loop from Theory to Practice.

Therefore, applying the control protocol designed in Section 3.1 to this scenario provides a distributed synchronous controller with prescribed transient performance and strong anti-disturbance capabilities for this network-type DER cluster. It not only ensures accurate synchronization of the DER cluster in steady state but also constrains the system's dynamic behavior within a safe and high-performance range that engineers can pre-design during dynamic recovery after disturbances. This provides a solid theoretical basis and feasible technical path for solving the stable operation problem of multi-DER systems during transient processes.

In a practical implementation, the proposed protocol serves as the high-level coordination layer, whose output reference is tracked by the local, fast inner-loop controllers of each inverter, which are responsible for managing the device's inherent higher-order dynamics and nonlinearities.

4 Simulation

Consider a network of $N = 5$ DERs, which was used in [12,25] to verify a cooperative control strategy. The core control dynamics of each DER are described by a first-order integrator model, whose states correspond to the internal phase angle variables of the equipment. The communication graph $\mathcal{G}$ of the multi-agent system is shown in Fig. 2. Let $p_i = [p_i^x, p_i^y]$ be internal phase angle variable of DER i, $i \in \{1, \cdots, N\}$, then the relative state of DER i is defined as $p_l^{\mathrm{x}} = p_i^{\mathrm{x}} - p_j^{\mathrm{x}}$ and $p_l^{\mathrm{y}} = p_i^{\mathrm{y}} - p_j^{\mathrm{y}}$, $\forall (i,j) \in \mathcal{E}$. Suppose the initial states of agents are $p_1 = [1.5\ 2.5]^\top$, $p_2 = [-1\ 1.3]^\top$, $p_3 = [1.6\ 0]^\top$, $p_4 = [1\ -2.7]^\top$, $p_5 = [-1\ -1.8]^\top$. It can be seen that $x_i \in \{p_i^{\mathrm{x}}, p_i^{\mathrm{y}}\}$ and $y_l \in \{p_l^{\mathrm{x}}, p_l^{\mathrm{y}}\}$, separately. The following simulations will be centered on the single-integrator dynamics system. For the following simulation experiments, we chose to perform them in the time interval from 0 to 3 s.

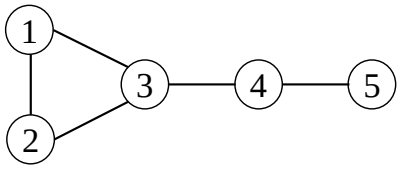


Figure 2: Communication graph $\mathcal{G}$ of five agents.

For the above multi-agent system, we select a same performance function for all edges

$$\rho_l(t) = (3 - 0.1)e^{-1.6t} + 0.1.$$

We choose the following communication perturbation, which occurs in the communication edge between two intelligences, i.e., a communication edge-based communication disturbances.

$$w_l(t) = \begin{cases} 20\sin(t), & 0 \le t \le 3, \\ 0.0, & \text{otherwise}, \end{cases} \tag{15}$$

For simplicity, the above perturbation holds for all communicating edges. According to Theorem 1, the multi-agent system with a prescribed performance control protocol (12) imposed is on each edge-based phase angle, i.e., on the relative phase angle. The results of our simulations for this scenario are shown in Figs. 3 and 4. In Fig. 3, it can be seen that the phase angle states of all DERs converge on the two-dimensional plane, reflecting the synchronization process of the output phases of each DER. In Fig. 4, it can be seen that under the condition of communication disturbance (15) on the communication edges, the relative phase angle trajectory evolves under the constraints of the prescribed performance boundary and eventually converges to zero, indicating that the system achieves phase synchronization.

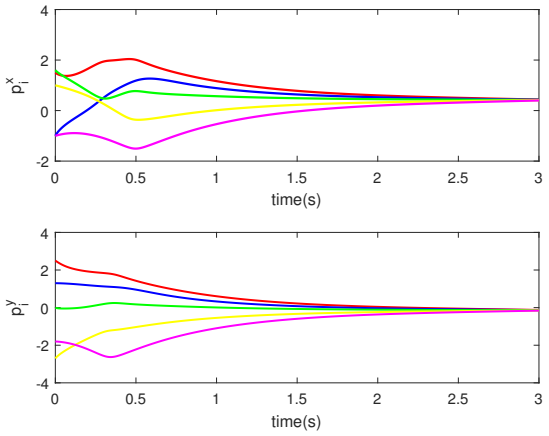


Figure 3: State trajectories of agents with PPC protocol (12) and disturbance (15).

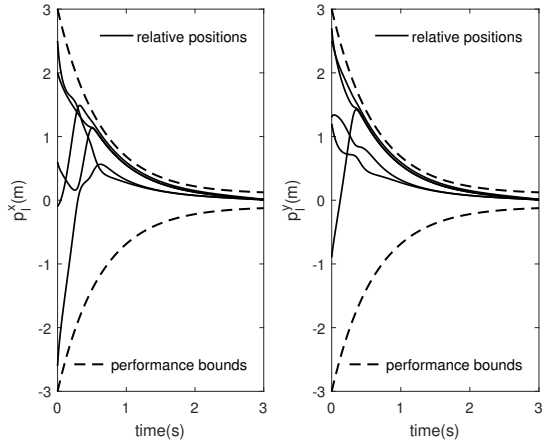


Figure 4: The trajectories of relative positions and performance bounds with PPC protocol (12) and disturbance (15), respectively.

As a comparison, we consider the case where no prescribed performance constraints are imposed and there are no edge-based communication perturbations, and the simulation results are shown in Fig. 5.

Compared to Fig. 4, we can see that it is difficult for the relative phase angle to converge to 0 quickly in the time interval from 0 to 3 s.

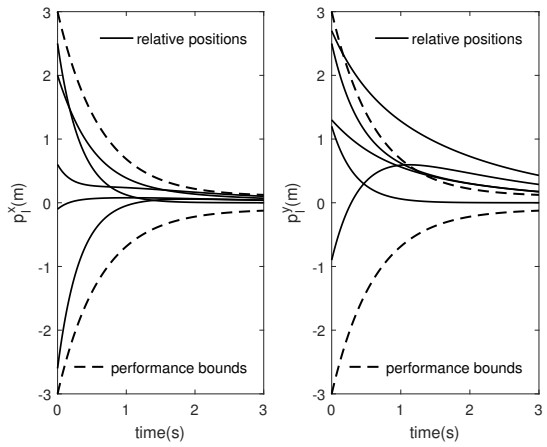


Figure 5: The trajectories of relative positions and performance bounds without PPC and disturbance, respectively.

Finally, we verified the effectiveness of the prescribed performance control protocol (12) in suppressing communication disturbance. For a more in-depth comparison, we did not impose prescribed performance constraints on the relative phase angle of the multi-DER systems, but still considered communication disturbance (15). The simulation results are shown in Fig. 6. It can be seen that under the influence of communication disturbance, the relative phase angle oscillates or even diverges, and synchronization is disrupted, rather than the convergence trend shown in Fig. 4. This simulates the risk of loss of synchronization of the multi-DER system in a microgrid under strong disturbance without effective control. The above sinusoidal-disturbance simulation verifies the effectiveness of Theorem 1 under the baseline communication disturbance. To further examine whether the proposed prescribed performance H_∞ control strategy remains effective under more realistic disturbance conditions, two additional simulations with impulsive and burst disturbances are presented below.

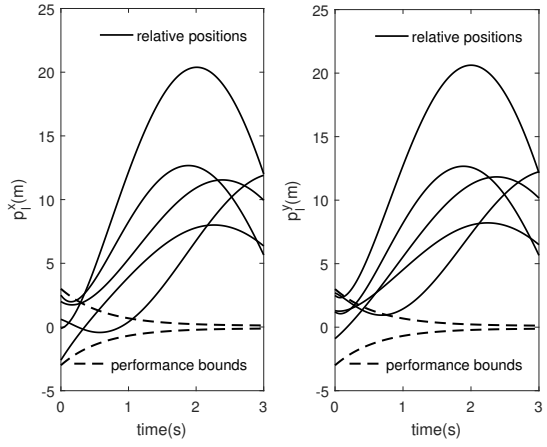


Figure 6: The trajectories of relative positions and performance bounds without PPC but with disturbance (15), respectively.

4.1 Additional Validation under Impulsive and Burst Disturbances

(a) Impulsive disturbance. The impulsive disturbance is constructed by superimposing Gaussian pulses onto the original signal, modeling abrupt shock-type interference:

$$w_l(t) = \begin{cases} 20\sin(t) + \sum_{k=1}^{3} A_k e^{-80(t-t_k)^2}, & 0 \le t \le 3, \\ 0, & \text{otherwise}, \end{cases} \tag{16}$$

where $t_1 = 0.5$ s, $t_2 = 1.5$ s, $t_3 = 2.5$ s and $A_1 = 30$, $A_2 = 50$, $A_3 = 40$. The Gaussian envelope $e^{-80(t-t_k)^2}$ concentrates each pulse's energy within a narrow window (width ≈ 0.2 s) around t_k, ensuring finite energy. The impulsive disturbance therefore satisfies the L_2 boundedness condition.

(b) Burst disturbance. The burst disturbance adds finite-duration high-frequency oscillations to model short-term intense disturbances:

$$w_l(t) = \begin{cases} 20\sin(t) + w_{\text{burst}}(t), & 0 \le t \le 3, \\ 0, & \text{otherwise}, \end{cases} \tag{17}$$

where

$$w_{\text{burst}}(t) = \begin{cases} 35\sin(16\pi(t-0.7)), & t \in [0.7, 1.0], \\ 50\sin(12\pi(t-1.8)), & t \in [1.8, 2.2], \\ 0, & \text{otherwise}. \end{cases}$$

Both segments have bounded amplitude and limited duration, with energies $\int_{0.7}^{1.0}[35\sin(16\pi(t-0.7))]^2 dt \approx 189.5$ and $\int_{1.8}^{2.2}[50\sin(12\pi(t-1.8))]^2 dt \approx 515.8$ respectively, so the burst disturbance also satisfies the L_2 boundedness condition.

The results under all three disturbance types are compared in Table 1. The performance function is $\rho(t) = (3-0.1)e^{-1.6t} + 0.1$ with $\rho(0) = 3.0$.

Table 1: Comparison of simulation results under three disturbance types.

Disturbance	Controller	$\max\lvert x_{ij}\rvert$	Instant	Edge	Within $\rho(t)$?
Sinusoidal	PPC	2.600	$t = 0$ s	Edge 3 (Agent 2↔3)	Yes
Sinusoidal	NoPPC	20.385	$t = 2.010$ s	Edge 1 (Agent 1↔3)	No
Impulse	PPC	2.600	$t = 0$ s	Edge 3 (Agent 2↔3)	Yes
Impulse	NoPPC	39.088	$t = 1.613$ s	Edge 1 (Agent 1↔3)	No
Burst	PPC	2.600	$t = 0$ s	Edge 3 (Agent 2↔3)	Yes
Burst	NoPPC	27.550	$t = 1.880$ s	Edge 1 (Agent 1↔3)	No

From Table 1, we can obtain two points as follows. First, with PPC control, the maximum $|x_{ij}|$ is 2.600 for all three disturbance types, well within $\rho(0) = 3.0$. This peak occurs at $t = 0$—the initial condition—rather than after the disturbance takes effect, confirming that the PPC controller confines the edge states within the prescribed region from the start and subsequently suppresses all disturbances. Second, without PPC (NoPPC), all three disturbances cause severe bound violations. The impulsive case is the worst, reaching

39.088 on Edge 1 (over 13× the initial bound); the burst case reaches 27.550 (over 9× the initial bound); the sinusoidal case reaches 20.385 (over 6.8× the initial bound). All uncontrolled maxima occur on Edge 1 (Agent 1↔3), indicating that this edge is the most sensitive to communication disturbances. Furthermore, the corresponding simulation results are shown in Figs. 7 and 8, which are consistent with the data in Table 1.

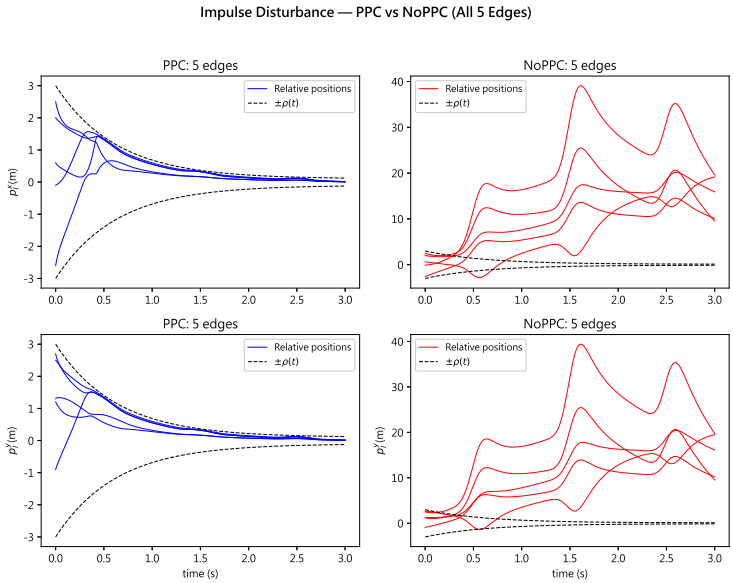


Figure 7: Comparison of relative positions under impulsive disturbance: PPC (left) vs. NoPPC (right). Dashed lines indicate the prescribed performance bound $\pm\rho(t)$.

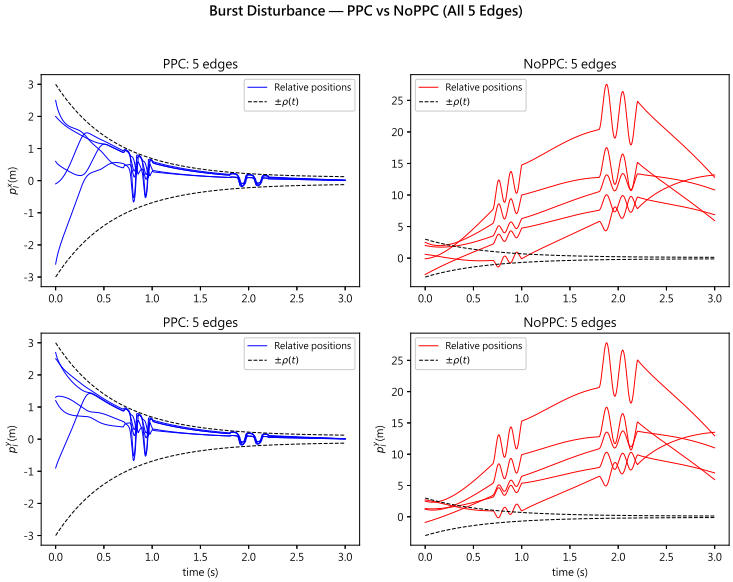


Figure 8: Comparison of relative positions under burst disturbance: PPC (left) vs. NoPPC (right). Dashed lines indicate the prescribed performance bound $\pm\rho(t)$.

In summary, the simulation results under three distinct types of finite-energy disturbances (sinusoidal, impulsive, and burst) consistently demonstrate that the proposed prescribed performance H_∞ control

strategy effectively rejects a broad class of communication disturbances while maintaining DER cluster synchronization. The inclusion of impulsive and burst cases further supports the method's applicability in real microgrid environments with complex electromagnetic interference.

4.2 Scalability and Benchmark Comparison

To further examine scalability, an additional 20-node ring-network simulation was conducted. Each DER communicates with two neighboring DERs, resulting in 20 communication edges. The initial states were randomly generated in $[-1.2, 1.2]$ using a fixed seed, and the maximum initial edge error satisfied $|e_{ij}(0)| < \rho(0)M = 3.0$. The simulation horizon was extended to 10 s with a step size of 0.005 s. Under sinusoidal, impulse, and burst disturbances, all edge errors under the proposed PPC+H_∞ controller remained within the prescribed boundary, with zero boundary violations and a maximum edge error of about 2.44. In contrast, pure consensus control without PPC produced edge errors of approximately 33–39 in the same 20-node setting.

We also compared the proposed controller with two baselines: a pure distributed consensus controller $\dot{x} = -Lx$ and a Riccati-based H_∞ consensus controller. The L_2 gain index $\gamma = \sqrt{\int \|e(t)\|^2 dt / \int \|w(t)\|^2 dt}$ was computed using the 5-node simulations under the three disturbance types. The proposed PPC+H_∞ controller achieved γ values below 0.07 in all cases, corresponding to average improvements of 13.08 times over pure consensus and 18.63 times over the H_∞ consensus controller. Furthermore, the corresponding simulation data are shown in Table 2. These results support both the scalability and the disturbance attenuation capability of the proposed method.

Table 2: H_∞ performance comparison: L_2 gain γ under three disturbance types.

Disturbance	Pure Consensus	H_∞ Consensus	PPC + H_∞	vs. Pure	vs. H_∞
Sinusoidal	0.6563	0.9359	0.0608	10.79×	15.39×
Impulse	0.5775	0.8215	0.0350	16.51×	23.49×
Burst	0.4733	0.6744	0.0397	11.93×	17.00×
Average improvement	–	–	–	13.08×	18.63×

5 Conclusion

In this article, prescribed performance H_∞ consensus of multi-DER systems under communication disturbances is investigated and realized. We consider the impact of edge-based communication disturbances and address the problem by means of a prescribed performance control method, which ultimately achieves H_∞ consensus. To expand the application scenarios, we briefly discuss the application of multi-DER system H_∞ consensus in a microgrid.

The proposed framework complements existing PPC-only and H_∞-only microgrid consensus methods. PPC-only methods provide explicit transient bounds but generally do not quantify disturbance attenuation for communication-link perturbations. H_∞-only methods improve robustness but do not prescribe the transient envelope of edge errors. By combining the two mechanisms, the proposed controller achieves prescribed transient performance and H_∞ consensus within one distributed framework.

The proposed distributed control protocol is inherently scalable as each DER relies solely on local neighbor information, with stability guarantees depending on graph connectivity rather than network size. The L_2-bounded disturbance model adopted, while standard for H_∞ analysis, encompasses various realistic perturbations including burst-type communication interruptions with finite energy. For practical deploy-

ment, key considerations involve balancing prescribed performance parameters with actuator constraints in large-scale systems and maintaining robustness against topology variations. Future work will explore more structured disturbance models and experimental validation in complex microgrid testbeds. A critical next step is the experimental validation of the proposed protocol on the physical microgrid testbeds to assess its performance under realistic communication delays, measurement noise, and hardware constraints.

To further validate the protocol, future simulation studies will explore its performance under more diverse conditions, including different network topologies, various disturbance types, and comparative analysis with other robust control methods.

Acknowledgement: Not applicable.

Funding Statement: The authors received no specific funding for this study.

Author Contributions: Study conception and design: Dongmei Wang, Huixin Song, Yanze Song; data collection: Dongmei Wang, Huixin Song, Yanze Song; analysis and interpretation of results: Dongmei Wang, Huixin Song, Yanze Song; draft manuscript preparation: Dongmei Wang, Huixin Song, Yanze Song. All authors reviewed the results and approved the final version of the manuscript.

Availability of Data and Materials: The data that support the findings of this study are available from the authors, upon reasonable request.

Ethics Approval: Not applicable.

Conflicts of Interest: The authors declare no conflicts of interest. The authors' professional appointments do not affect the research or publication of this work.

Nomenclature

Abbreviation	Full Term
DER	Distributed Energy Resource
PPC	Prescribed Performance Control
MAS	Multi-Agent System
H_∞	H-Infinity (Control)
$\mathcal{G}$	Communication Graph
$\mathcal{V}$	Set of Nodes/Agents
$\mathcal{E}$	Set of Communication Edges
$\rho_l(t)$	Prescribed Performance Function
L_2	Space of Square-Integrable Functions (Finite-Energy Signals)

References

1. Li Y, Tan C. A survey of the consensus for multi-agent systems. Syst Sci Control Eng. 2019;7(1):468–82. [CrossRef]
2. Izmirlioglu Y, Pham L, Son TC, Pontelli E. A survey of multi-agent systems for smartgrids. Energies. 2024;17(15):3620. [CrossRef]
3. Qin J, Ma Q, Yang S, Long W. Recent advances in consensus of multi-agent systems: a brief survey. IEEE Trans Ind Electron. 2017;64(6):4972–83. [CrossRef]
4. Zhang XM, Han QL, Ge X, Ding D, Ding L, Yue D, et al. Networked control systems:a survey of trends and techniques. IEEE/CAA J Autom Sin. 2020;7(1):1–17. [CrossRef]
5. Kong M, Peng X, Li Z, Shen F, Liu Y, Zhong W. Asynchronous double consensus-based distributed optimization for sustainable industrial utility systems. Energy. 2025;331:136630. [CrossRef]
6. Dai X, Liu GP, Hu W, Deng Q. Consensus-based secondary control for DC microgrids with communication delays via a networked predictive control strategy. ISA Trans. 2024;148:387–96. [CrossRef]

7. Singhal A, Vu TL, Du W. Consensus control for coordinating grid-forming and grid-following inverters in microgrids. IEEE Trans Smart Grid. 2022;13(5):4123-33. [CrossRef]
8. Bechlioulis CP, Rovithakis GA. Robust adaptive control of feedback linearizable MIMO nonlinear systems with prescribed performance. IEEE Trans Autom Control. 2008;53(9):2090–9. [CrossRef]
9. Karayiannidis Y, Doulgeri Z. Model-free robot joint position regulation and tracking with prescribed performance guarantees. Robot Auton Syst. 2012;60(2):214–26. [CrossRef]
10. Sun Z, Gao Z, Guo G, Wen S. Finite-time control of vehicular platoons with global prescribed performance and actuator nonlinearities. IEEE Trans Intell Veh. 2023;9(1):1768–79. [CrossRef]
11. Shao S, Chen M. Adaptive neural discrete-time fractional-order control for a UAV system with prescribed performance using disturbance observer. IEEE Trans Syst Man Cybern Syst. 2021;51(2):742–54. [CrossRef]
12. Chen F, Dimarogonas DV. Leader-follower formation control with prescribed performance guarantees. IEEE Trans Control Netw Syst. 2021;8(1):450–61. [CrossRef]
13. Soofi M, Jalilvand A, Delavari H, Mobayen S, Su CL. Prescribed performance control strategy for an isolated multi-agent DC microgrid. IEEE Trans Smart Grid. 2025;16(1):62–73. [CrossRef]
14. Zaery M, Amrr SM, Ali M, Hussain SMS, Abido MA. Prescribed performance-based distributed predefined time control for DC microgrid clusters. IEEE Trans Circuits Syst I Regul Pap. 2025;72(10):6262–75. [CrossRef]
15. Yuan QF, Wang YW, Liu XK, Liu ZW. Prescribed performance-based secondary control for DC microgrid. IEEE Trans Energy Convers. 2022;37(4):2610–9. [CrossRef]
16. Li W, Xu Z, Chen M, Wu Q. Distributed cooperative control for DC microgrids: a prescribed-time consensus method. Energy Rep. 2025;14:792–802. [CrossRef]
17. Dong X, Zhang H, Xie X, Ming Z. Data-driven distributed H_∞ current sharing consensus optimal control of DC microgrids via reinforcement learning. IEEE Trans Circuits Syst I Regul Pap. 2024;71(6):2824–34. [CrossRef]
18. Raeispour M, Atrianfar H, Baghaee HR, Gharehpetian GB. Resilient H_∞ consensus-based control of autonomous AC microgrids with uncertain time-delayed communications. IEEE Trans Smart Grid. 2020;11(5):3871–84. [CrossRef]
19. Zhou J, Xu Y, Sun H, Wang L, Chow MY. Distributed event-triggered H_∞ consensus based current sharing control of DC microgrids considering uncertainties. IEEE Trans Ind Inform. 2020;16(12):7413–25. [CrossRef]
20. Zhao Q, Zhang W, Zhang T, Chen J, Ye H. Robust consensus-based secondary control for microgrids considering communication delay and noises: a kalman filter-based approach. IEEE Trans Smart Grid. 2025;16(4):2791–802. [CrossRef]
21. Bu X, Wu X, Zhu F, Huang J, Ma Z, Zhang R. Novel prescribed performance neural control of a flexible air-breathing hypersonic vehicle with unknown initial errors. ISA Trans. 2015;59:149–59. [CrossRef]
22. Jiang T, Huang J, Li B. Composite adaptive finite-time control for quadrotors via prescribed performance. J Frankl Inst-Eng Appl Math. 2020;357(10):5878–901. [CrossRef]
23. Stamouli CJ, Bechlioulis CP, Kyriakopoulos KJ. Robust dynamic average consensus with prescribed transient and steady state performance. Automatica. 2022;144:110503. [CrossRef]
24. Uddin M, Mo H, Dong D, Elsawah S, Zhu J, Guerrero JM. Microgrids: a review, outstanding issues and future trends. Energy Strategy Rev. 2023;49:101127. [CrossRef]
25. Wu F, Lian J, Wang D, Zhai G. Prescribed performance bumpless transfer control for switched large-scale nonlinear systems. IEEE Trans Syst Man Cybern Syst. 2023;53(8):5139–48. [CrossRef]